Adaptive Self-Assembly in 2D Nanoconfined Spaces: Dealing with Geometric Frustration

Lander Verstraete,[1] Pawel Szabelski,[2] Ana M. Bragança,[1] Brandon E. Hirsch,[1] and Steven De Feyter*[1]

[1] Department of Chemistry, Division of Molecular Imaging and Photonics, KU Leuven, Celestijnenlaan 200F, B-3001 Leuven, Belgium.

[2] Department of Theoretical Chemistry, Faculty of Chemistry, Maria Curie-Sklodowska University, Pl. M.C.Sklodowskiej 3, 20-031 Lublin, Poland

Abstract

The impact of lateral confinement on the 2D self-assembly of a normal alkane is investigated *via* scanning tunneling microscopy-based nanoshaving on covalently modified graphite surfaces. Physical constraints placed on the confined assemblies lead to geometric frustration, which is shown to be released *via* a suppression of the lamellar order. This result is explained on the basis of competing enthalpic contributions from molecule-molecule and molecule-substrate interactions, and is corroborated by a simple coarse grain model. Furthermore, a pronounced molecular alignment effect results from the *in situ* nanoshaving procedure.

Introduction

Spatial confinement often has major implications for molecular ordering processes, and drastically changes the material properties. For example, crystallization of small molecules inside porous templates impacts nucleation rate,[1, 2] polymorph stability,[3-5] and growth orientation.[6, 7] Typically, phase transitions of these confined crystals are notably affected. As a general rule, melting and freezing points are depressed for smaller crystallite dimensions.[8, 9] These pronounced spatial confinement effects are ascribed to the larger surface-to-bulk ratio, and a lower degree of freedom of molecular motion. In addition, specific interactions between the confined molecules and the container walls can greatly influence their properties.[10, 11]

Analogous to crystallization confined within nanoporous templates, the formation of monolayer thin films can be significantly impacted by lateral confinement. For instance, the molecular packing arrangement is known to depend on the surface terrace area.[12] Similarly, the time required to form ordered, stable assemblies in nanoscale, shallow etch pits, is reported to depend on the pit area.[13, 14] Nevertheless,

while informative, these studies did not report on the role of confinement geometry since the shape of surface terraces and etch pits can hardly be controlled.

Drawing on the nanoshaving procedure reported by Xu *et al.* and others,[15-17] we recently developed an approach to create laterally restricted spaces with well-defined geometry on the surface of covalently modified highly oriented pyrolytic graphite (CM-HOPG).[18] In our approach, the HOPG surface is covalently modified with a dense layer of aryl species, which are locally removed by means of scanning tunneling microscopy (STM) nanoshaving. During nanoshaving, the STM tip is operated in close proximity to the surface, thereby raising the mechanical force on the grafted aryl species and detaching them from the surface. Using this procedure, areas of pristine graphite, *i.e.* corrals, are created and their geometry and orientation with respect to the substrate underneath, can be accurately controlled. We have shown that self-assembly in such corrals may go hand in hand with a strong molecular alignment effect when the shaving is performed *in situ, i.e.* in the presence of solute molecules,[19, 20] ultimately leading to the biased formation of selected enantiomorphous domains.[21] Furthermore, this approach also revealed nanocorral size-dependent polymorphism.[22] However, all of the molecules investigated so far are rather complex in nature, and their assemblies are dictated by directional, and often strong intermolecular interactions.

Normal alkanes (n-alkanes), *i.e.* linear saturated hydrocarbons, are undoubtedly one of the most basic molecular components. On solid supports such as graphite,[23] noble metals,[24, 25] and transition metal dichalcogenides,[26] n-alkanes spontaneously form ordered 2D monolayers, stabilized solely by weak van der Waals forces. On the basal plane of graphite, n-alkanes adopt a close-packed lamellar arrangement with the carbon backbone fully extended in an all-trans conformation, as inferred from STM imaging. These images are typically interpreted according to Groszek's model of commensurate registry on the graphite surface.[27] In this model, the alkane backbone is adsorbed parallel to the surface, with the chain extending along the graphite zigzag direction. From medium to long chain alkanes, similar arrangements have been observed, characterized by long-range ordered lamellae.[28, 29] Instigated by the impact of lateral confinement on 2D self-assembly, we set out to investigate how such confinement affects the formation of n-alkane monolayers, as part of a larger research effort.

In this work, we examine the impact of lateral confinement on the self-assembly of n-pentacontane (n-$C_{50}H_{102}$) at the phenyloctane-graphite interface. n-$C_{50}H_{102}$ was chosen for two reasons: first, n-$C_{50}H_{102}$ is known to form well-ordered monolayers on the basal plane of graphite;[30-33] and second, the relatively long alkane chain is expected to be quite susceptible to confinement effects due to the weak non-covalent interactions involved in the self-assembly. To realize controlled lateral confinement, STM nanoshaving is performed on a graphite surface that is covalently decorated with a dense layer of 3,5-bis-*tert*-butylaryl species (Figure 1a). Nanoshaving is performed *in situ* (in the presence of a n-$C_{50}H_{102}$ solution) rather than

ex situ (n-$C_{50}H_{102}$ solution added after corral fabrication) since the former is more practical, thus allowing interrogation of a statistically meaningful number of corrals. Comparison of n-$C_{50}H_{102}$ assemblies on bare graphite with assemblies inside host nanocorrals reveals a strong alignment of n-$C_{50}H_{102}$ chains along the fast shaving axis, in line with previous studies. Furthermore, by studying different corral shapes, we demonstrate how geometric frustration affects the degree of lamellar order (Figure 1b). These results are finally tested against a simple coarse grain model.

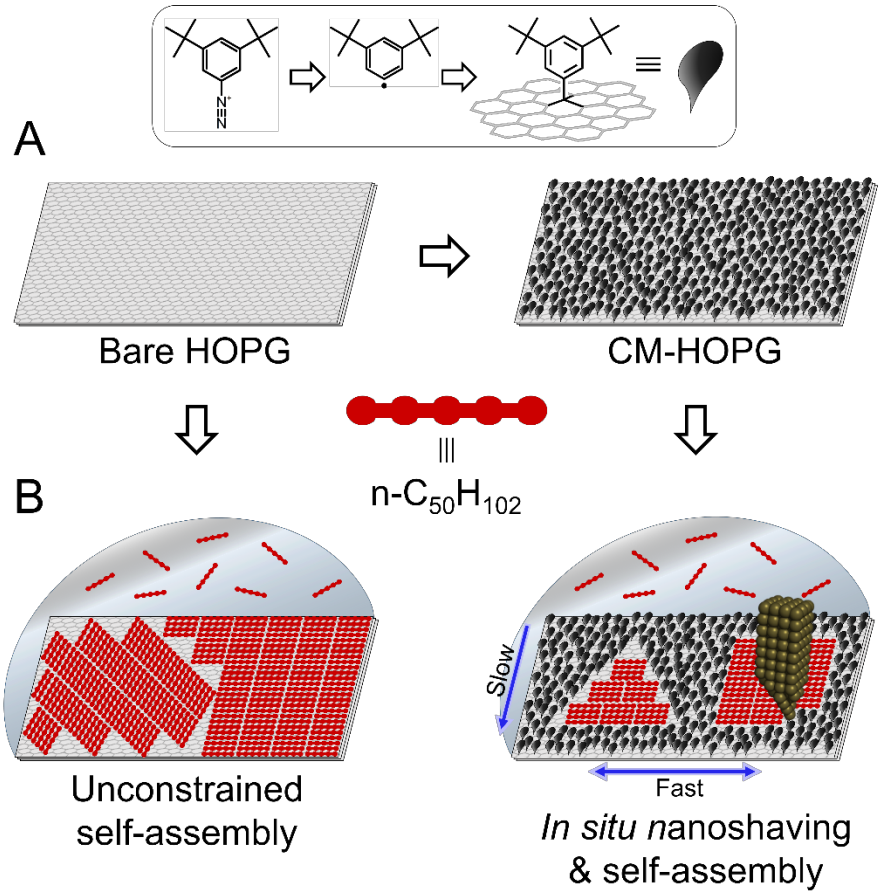

Figure 1. Schematic illustration of (a) the electrochemical grafting process, and (b) n-$C_{50}H_{102}$ self-assembly at the solution-graphite interface. Unconstrained self-assembly is characterized by the formation of straight lamellae with long-range order. Self-assembly inside *in situ* created nanocorrals displays a less ordered packing arrangement depending on the geometry of the exposed area.

Experimental section

STM experiments. All STM experiments were performed on a PicoLE (Keysight) setup operated in constant current mode at room temperature (20-22 °C). STM tips were prepared by mechanical cutting from Pt/Ir wire (Advent Research Materials, 80%/20%, diameter 0.25 mm). A 10^{-4} M solution of n-$C_{50}H_{102}$

(Sigma-Aldrich, ≥ 97%) in 1-phenyloctane (J&K Scientific, 99%) was dropcasted on the surface of freshly cleaved or covalently modified HOPG (grade ZYB, Advanced Ceramics Inc., Cleveland, OH, USA). When indicated in the figure caption, the high resolution STM images were corrected for thermal drift using a reference image of the graphite lattice recorded under the same conditions, except for I_t = 200 pA, V_s = -0.001 V. All images were processed using the Scanning Probe Imaging Processor (SPIP) software (Image Metrology ApS). Imaging parameters are given in the figure captions and are denoted by I_t for the tunneling current, and V_s for the sample bias.

Covalent modification of HOPG. 3 mg 3,5-bis-*tert*-butylaniline (TCI, >98%) was dissolved in 5 mL aqueous hydrochloric acid (Honeywell-Fluka, 50 mM). To start the diazotization reaction, 100 µL of aqueous $NaNO_2$ (Sigma-Aldrich, 99.999%, 0.1 M) was added, and the solution was shaken for 90 s. Then, the solution was poured into a lab-built single-compartment thee-electrode cell (HOPG working electrode, 38.5 mm^2; Pt wire counter electrode; Ag/AgCl/3 M NaCl reference electrode). The diazonium species were electrochemically reduced *via* cyclic voltammetry controlled by an Autolab PGSTAT101 potentiostat (Metrohm_Autolab BV, The Netherlands). Each experiment consisted of three voltage cycles from 0.6 V to -0.35 V, with a scan rate of 0.1 V/s (Figure S1). After modification, the surface was rinsed with Milli-Q water. All aqueous solutions were prepared with Milli-Q water (Millipore, 18.2 MΩ cm, TOC < 3 ppb).

Nanoshaving. Nanoshaving was performed in a line-wise fashion, with the fast shaving direction orthogonal to the slow shaving direction. The tip speed was set to 2 µm/s, and the tunneling conditions were I_t = 200 pA; V_s = -0.001 V. The vertical spacing between consecutive lines varied from 0.3 nm to 0.4 nm. The corral geometry was controlled using the PicoLITH v.2.1 software package. Statistics on alignment inside *in situ* square nanocorrals were obtained considering only the predominant assembly orientation (*i.e.* the rotational domain occupying the largest area) in case of multiple rotational domains. In *ex situ* squares, the surface coverage for each rotational domain was measured and normalized to the total corral area.

Coarse grain simulations. The simulations were performed on a square lattice on which an equilateral triangular active zone of base equal to 51 sites was delimited. The adsorbing molecules were represented by five connected segments forming a rigid rod-like structure having length $l = 5$. Each molecular segment was allowed to occupy one site of the lattice. The molecules were assumed to interact *via* the attractive interaction potential U_{ij} defined in Fig. 5A (vanishing for $r \geq l$). The simulations were performed assuming that desorption of the molecules can be neglected, that is the molecules were sequentially deposited and the resulting assembly was equilibrated using the conventional MC method in the canonical ensemble. To that end, in the first step of the simulation, a molecule was deposited inside the triangular zone, parallel to the base. Next a series of MC steps was performed in which position of each adsorbed molecule was changed by moving it randomly vertically or horizontally by one lattice site. To

accept new molecular configuration, the interaction energy in the old position, E_o was calculated using the potential function U_{ij} and it was compared with the analogous value, E_o obtained for the new position. Next, the acceptance probability $p = \min[1, \exp\left(-\frac{\Delta E}{kT}\right)]$ was calculated, where $\Delta E = E_n - E_o$ and k is the Boltzmann constant, and it was compared with a randomly generated number $\alpha \in (0,1)$. If α was smaller than p the new configuration was accepted; otherwise the molecule was left in the original (old) position. The simulated structures were obtained using 10^5 attempts to insert a molecule, and each successful insertion was followed by 10^4 equilibration steps (see above) per one adsorbed molecule. The energies and temperatures in our model are expressed in units of ε and ε/k, respectively.

Results and discussion

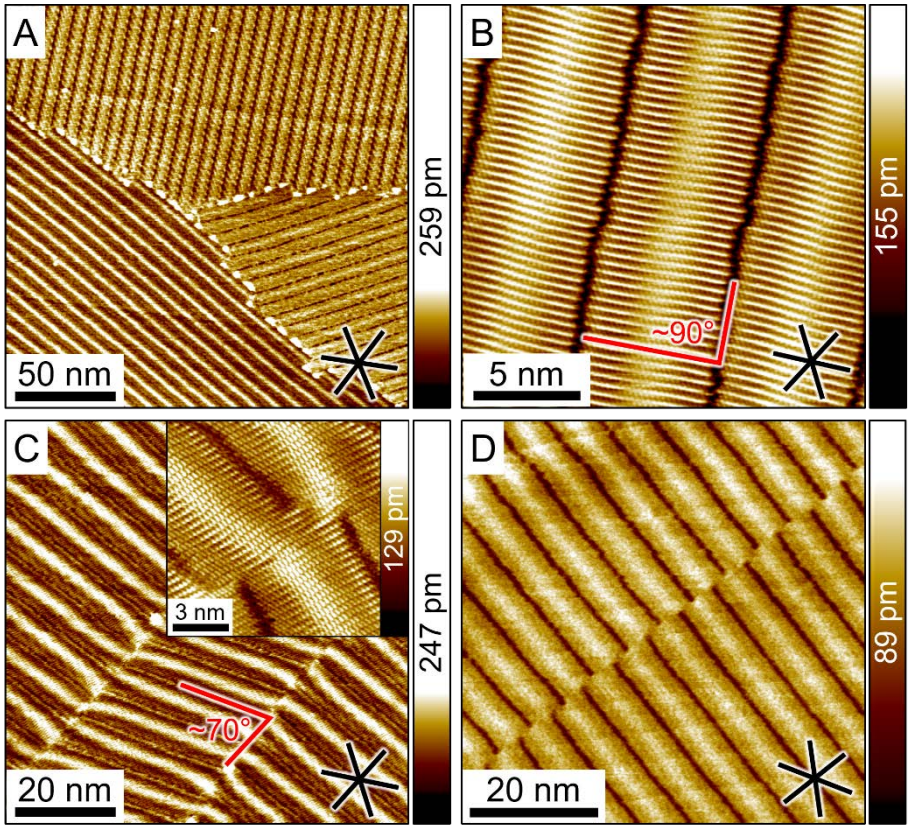

Figure 2. Scanning tunneling microscopy topography images of a n-$C_{50}H_{102}$ monolayer at the phenyloctane-graphite interface. (a) Long-range ordered lamellae are observed to run perpendicular to the high symmetry axes of graphite (black axes). (b) High resolution image showing the arrangement of individual alkane chains. Each chain is aligned along the high symmetry direction of graphite, and is oriented perpendicular to the lamellar direction. (c) Observation of tilted lamellae deviating ~20° from the preferred lamellar orientation. Inset: high resolution image obtained at the border between straight (bottom) and tilted (top)

lamellae. The alkane chains are adsorbed along the high symmetry axes of graphite for both straight and tilted lamellae. (d) Phase shift defect interrupting the long-range lamellar order. Image (b), and the inset in (c) were corrected for thermal drift. Imaging conditions: (a,c) I_t = 140 pA, V_s = -0.8 V; (b) I_t = 200 pA, V_s = -0.8 V; (d) I_t = 120 pA, V_s = -0.8 V.

Initially, self-assembled monolayers of n-$C_{50}H_{102}$ were characterized on bare HOPG to serve as a benchmark for future comparison with self-assembled structures inside the confined spaces of nanocorrals. As shown in Figure 2a, n-$C_{50}H_{102}$ organizes at the phenyloctane-HOPG interface in straight lamellae that extend over hundreds of nanometers. The markedly different contrast features for separate rotational domains in Figure 2a are attributed to a scanning artefact, *i.e.* the lamellar orientation with respect to the fast scan axis. A high resolution image, as shown in Figure 2b, reveals that individual alkane chains lie along the graphite high symmetry axes (zigzag direction) and are oriented perpendicular to the inter-lamellar troughs. The lamellar width and inter-chain distance were determined to be 6.55 ± 0.05 nm and 0.43 ± 0.01 nm, respectively. Interestingly, the inter-lamellar troughs, as seen from Figure 2b, are observed to be slightly jagged, indicating a certain degree of disorder at the level of individual alkane chains. This disorder is dynamic (Figure S2) and is attributed to minute displacements of neighboring alkane chains along the molecular axis, and desorption of chain ends. Such a loose packing arrangement exists due to the weak, non-directional van der Waals interactions that stabilize the assembly.

Occasionally, defects in the packing arrangement were observed. For instance, tilted lamellae were encountered as shown in Figure 2c. In this case, the alkane chains remain aligned along the high symmetry axes of graphite (Figure 2c, inset), but are oriented at an oblique angle with respect to the inter-lamellar troughs. On average, a molecule-trough angle of 71.6° ± 3.5° was found from 24 measurements on tilted lamellae. Tilted lamellae of n-alkanes have been observed on Au surfaces,[34] as well as on HOPG for shorter n-alkanes,[35-37] but the molecule-trough angle was consistently reported to be close to 60°. In the present case, the tilted lamellae are believed to represent a metastable arrangement. This is supported by the observation of a reorganization into straight lamellae over time (Figure S3). Furthermore, another type of packing defect arises from a discrete translational offset along the molecular axis (Figure 2d). Following the crystallographic terminology, this type of defect is referred to a phase shift defect. Despite disrupting the long-range lamellar order, such phase shift defects were found to be stable for long durations (>25 min, Figure S3).

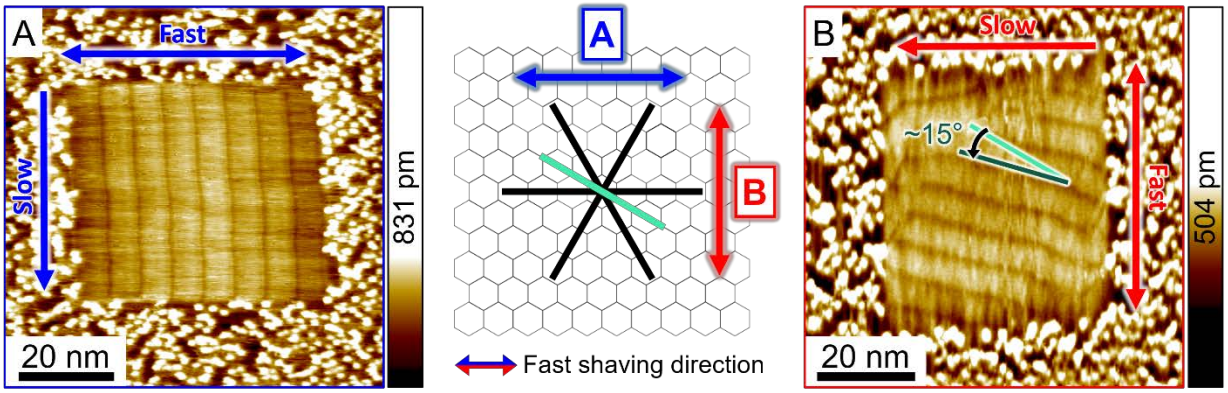

Figure 3. Scanning tunneling microscopy images showing n-$C_{50}H_{102}$ self-assembly inside square nanocorrals created with the fast shaving direction (a) parallel, and (b) orthogonal to one of the high symmetry axis of graphite (black axes). In case (a), straight lamellae containing n-$C_{50}H_{102}$ chains adsorbed parallel to the fast shaving direction are preferred. In case (b), the alkane chains are preferably adsorbed along a symmetry axis oriented at 30° with respect to the fast shaving direction, but the lamellae tend to be tilted towards the corral border. The actual lamellar direction in (b) (dark green line) deviates by approximately 15° from the expected direction for straight lamellae (light green line). Imaging conditions: (a,b) I_t = 60 pA, V_s = -0.8 V.

To probe the impact of lateral confinement on the self-assembly of n-$C_{50}H_{102}$, nanocorrals were *in situ* created at the solution-solid interface. To begin with, square corrals were created with the fast nanoshaving direction carefully oriented parallel to one of the high symmetry axes of graphite (Figure 3, case a). As shown in Figure 3a, the square corrals are completely filled with n-$C_{50}H_{102}$ lamellae. The lamellae are generally straight, although a certain degree of disorder in the inter-lamellar troughs is inevitably present. Interestingly, in 88 of the 89 investigated corrals, the n-$C_{50}H_{102}$ chains were predominantly oriented parallel to the fast shaving direction. Next, square nanocorrals were fabricated with the fast shaving direction perpendicular to one of the high symmetry axes of graphite (Figure 3, case b). Under these conditions, registry with the substrate forbids adsorption of the n-$C_{50}H_{102}$ chains parallel to the fast shaving direction. Instead, the alkane chains were found to be predominantly oriented at an angle of 30° with respect to the fast shaving direction (49 out of 50 corrals). Surprisingly though, in this case, the lamellae display a strong propensity to tilt towards the nanocorral border. This behavior is illustrated in Figure 3b, which shows that the lamellae are tilted approximately 15° towards the bottom border. The tendency to tilt towards the border suggests a high degree of geometric frustration exerted on the assemblies. Additional examples of “case a” and “case b” corrals are provided in Figure S4.

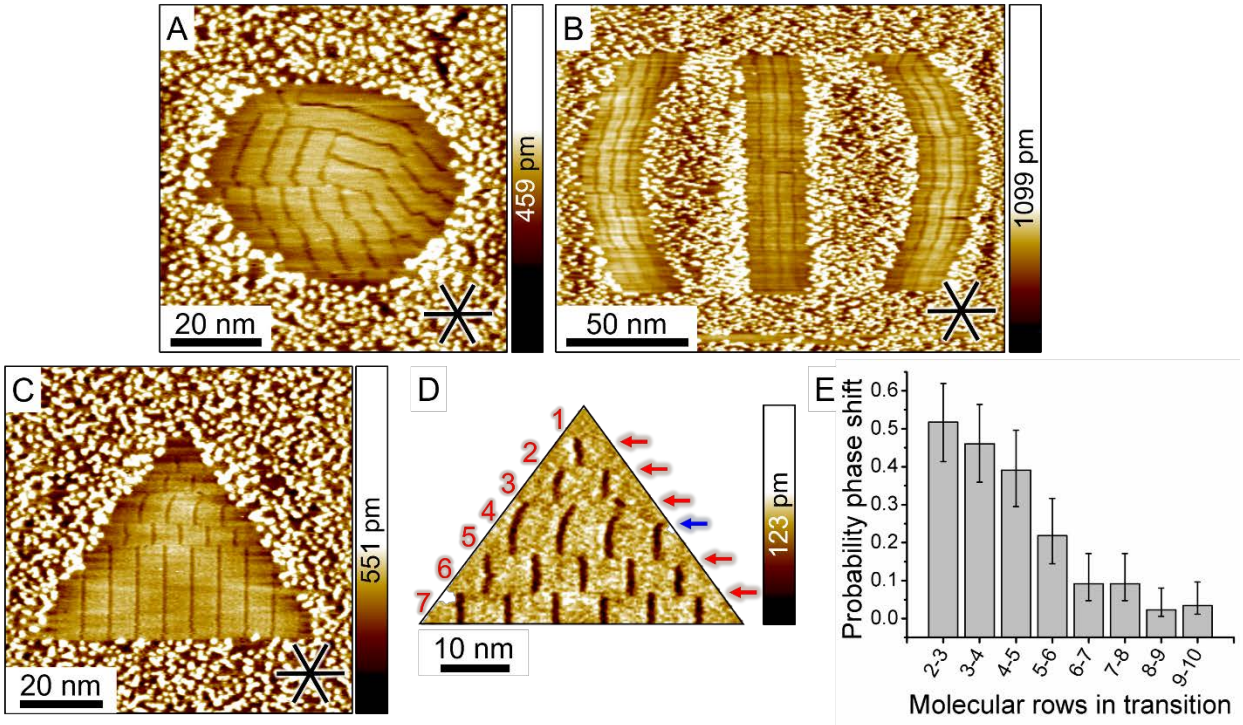

Figure 4. Scanning tunneling microscopy images showing self-assembly of n-$C_{50}H_{102}$ inside a series of *in situ* created nanocorrals of different shapes: (a) disc, (b) narrow trenches, and (c) triangle. For each shape, nanoshaving was performed from top to bottom, with the fast shaving direction parallel to one of the high symmetry axes of graphite (black axes). (d) Zoomed image near the apex of the triangular corral shown in (c). The vertical position of phase shift defects is indicated by red arrows. The transition between 4 and 5 lamellae proceeds without a phase shift defect (blue arrow). (e) Probability of phase shift defects *vs.* the number of molecular rows involved in the transition (87 triangular corrals investigated). The error bars represent 95% Wilson score intervals. Imaging conditions: (a) I_t = 70 pA, V_s = -0.8 V; (b,c) I_t = 60 pA, V_s = -0.8 V.

The impact of geometric frustration on the lamellar ordering of n-$C_{50}H_{102}$ was further probed by changing the corral shape. From here on, the fast nanoshaving direction is consistently oriented parallel to a graphite high symmetry axis. For disk-shaped nanocorrals, the complete corral area was again completely filled with n-$C_{50}H_{102}$ lamellae that were predominantly aligned (Figure 4a, Figure S5). However, compared with "case a" square nanocorrals, tilted lamellae and phase shift defects were more commonly found in discs, as evident from Figure 4a. Clearly, the loss of lamellar order in disc-shaped corrals is related to the curvature of the corral boundaries. To demonstrate this more clearly, an image containing both linear and curved trenches of just a few lamellae wide was created (Figure 4b). As anticipated, the self-assembled n-$C_{50}H_{102}$ lamellae adapt to the curvature of the trench borders to deal with the geometric frustration.

Given the remarkable ability to adapt to curved structures, we wondered how n-$C_{50}H_{102}$ would assemble inside triangular corrals. A series of equilateral triangles was created and a pattern as the one shown in Figure 4c was typically encountered. The number of molecular rows is seen to vary with triangle width, and the transitions are often accompanied with the incorporation of a phase shift defect. However, phase shift defects do not consistently occur with every transition. For instance, in Figure 4c (and the zoom in Figure 4d), when going from four to five lamellae no phase shift is observed. Rather, the lamellae tilt slightly to the left in order to allow incorporation of an additional row on the right (blue arrow). Similarly, the transition from seven to nine molecular rows in Figure 4c proceeds without defects. To check whether a relation exists between the formation of phase shift defects and triangle width, we monitored, for a total of 87 corrals, the frequency of phase shift defects as a function of the number of lamellae involved in the transition. As shown in Figure 4e (and Figure S6), a clear dependence on the vertical position inside the triangle is displayed: near the triangle apex, with space for only a few lamellae, phase shift defects emerge with high probability, but the likelihood of their appearance decreases steadily towards the bottom of the triangle. This result suggests a subtle balance between lamellar ordering on the one hand, and defect incorporation as a result of geometric frustration on the other hand.

The alignment of molecules during *in situ* nanoshaving has previously been observed for alkylated molecules, and is believed to be mediated by lateral constraints during the initial stages of nanoshaving, and an interaction of the assembling molecules with the STM tip during the shaving process. This is further corroborated by the absence of a pronounced alignment effect inside *ex situ* created corrals, *i.e.* corrals created on dry CM-HOPG substrates prior to the addition of n-$C_{50}H_{102}$ solution (Figure S7). Based on the current findings, we hypothesize that molecular alignment during *in situ* nanoshaving applies more generally to linear, alkylated molecules. However, previous experiments did not reveal a discernible impact on the degree of ordering attained by the confined assemblies. This difference is attributed to the lack of strong, directional interactions in the case of n-$C_{50}H_{102}$ self-assembly. Our results also agree well with the impact of spatial confinement on the 3D crystallization behavior of n-alkanes. Indeed, crystallization studies in various size-restricted environments revealed that, compared to bulk crystallization, confinement tends to favor disordered phases as evidenced by depressed melting/freezing points,[38-40] occurrence of amorphous phases,[41] stabilization of rotator phases,[39, 42, 43] and suppression of phase separation in binary mixtures.[44] These results corroborate the fact that alkanes are particularly susceptible to spatial confinement owing to their weak intermolecular interactions.

An important question pertaining to the observed assembly features of n-$C_{50}H_{102}$ inside nanocorrals is the nature of stabilization provided by spatial confinement. From a kinetics' point of view, the gradual revelation of pristine graphite during *in situ* nanoshaving might strongly determine the self-assembly

conditions. For instance, in the case of triangles, one might wonder whether the observed pattern of phase shift defects is not merely a consequence of a gradual filling of the exposed corral area. Once formed, these structures can be kinetically trapped inside the confined spaces. To rule out this scenario, nanoshaving of triangular corrals was performed *ex situ.* Again a pattern of phase shift defects was observed (Figure S8) similar to the results obtained *via* an *in situ* nanoshaving approach. Furthermore, long-term imaging (> 60min) of n-$C_{50}H_{102}$ inside *in situ* created triangular corrals revealed that phase shift defects remain stable over time (Figure S9), and occasionally the formation of additional phase shift defects was observed (Figure S10). Overall, these results provide strong evidence that the formation of phase shift defects near the triangle apex, is energetically favored. Likewise, tilting of lamellae in response to corral borders is believed to be energetically driven.

From a thermodynamics' perspective, the suppression of lamellar order inside nanocorrals can be rationalized by a competition between molecule-substrate and molecule-molecule interactions. On the one hand, molecule-substrate interactions are additive, and the associated enthalpic gain increases with the number of molecules adsorbed on the surface. Molecule-molecule interactions, on the other hand, are optimized when well-ordered, straight lamellae are formed. In square corrals created with the fast shaving direction parallel to a graphite high symmetry axis (case a), no competition exists since straight lamellae fit geometrically well. However, when the shaving direction for square corrals is rotated (case b), or inside disc-shaped and triangular spaces, the number of adsorbed molecules can only be maximized when lamellar order is lost. This competition is especially apparent from triangular corrals. Near the triangle apex, the high number of phase shift defects implies that maximum surface occupation prevails over optimal intermolecular interactions. However, as the triangle width increases, more molecular rows fit and the energy penalty per phase shift defect increases. Eventually, the balance is shifted in favor of optimal molecule-molecule interactions, thus explaining the lower number of phase shift defects near the base of the triangle. In an analogous fashion, tilting of lamellae in response to curved corral borders can be interpreted as driven by molecule-substrate interactions favoring complete filling over well-ordered lamellae. Our experimental observations can thus be well explained on the grounds of a competition between different enthalpic contributions. From this account, it also follows that weak intermolecular interactions with respect to the molecule-substrate interactions are crucial to observe an efficient suppression of lamellar ordering.

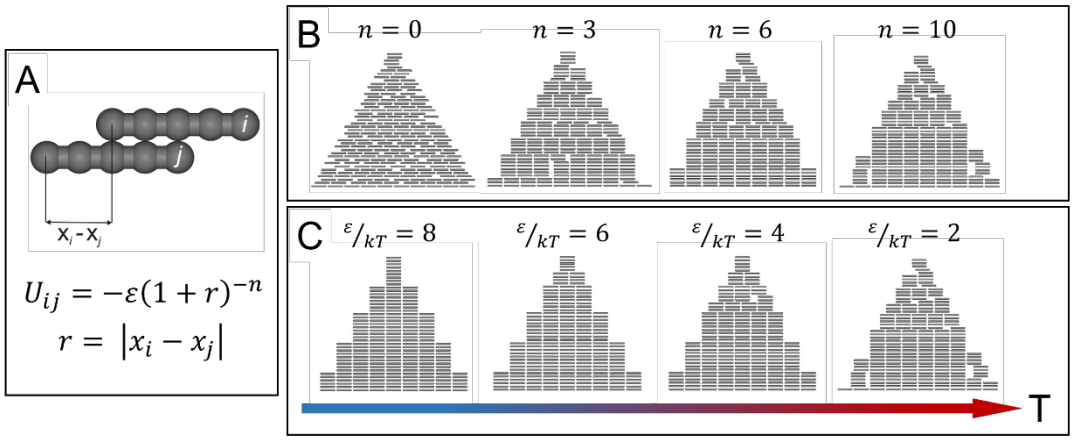

Figure 5. (a) Description of the coarse-grain model used to mimic self-assembly of n-$C_{50}H_{102}$. (b) Snapshots of self-assembled n-$C_{50}H_{102}$ patterns confined within equilateral triangular geometries. Different power dependencies of the interaction potential are shown, with ε/kT = 2. (c) Snapshots obtained for different values of ε, with n = 10. Lower ε/kT values correspond to weaker intermolecular interactions or higher temperatures.

A simple coarse-grain model was developed in order to test the assumption of competitive interactions in confined spaces. In this model, n-$C_{50}H_{102}$ is simplified as five segments on a string, and the interaction potential between neighboring molecules is dependent on their relative horizontal shift (Figure 5a). Self-assembly of n-$C_{50}H_{102}$ was simulated in equilateral triangles for different power dependencies (n) of the interaction potential and different intermolecular interaction strengths (ε). In contrast to our experimental approach, the complete corral area was exposed from the start of the simulation. This simplification seems justified since similar behavior was observed for both *in situ* and *ex situ* shaving procedures. Furthermore, molecular adsorption was restricted to a single orientation. When n = 0, no enthalpic driving force for lamellar ordering exists, leading to a random filling of the corral area as shown in Figure 5b. Therefore, a more realistic situation is represented by non-zero values of n. Whether or not lamellae are interrupted by phase shift defects depends on the shape of the interaction potential (n), with larger values of n leading to fewer phase shift defects. Interestingly, for increasing n, phase shift defects first disappear near the base of the triangle. Furthermore, simulations for varying values of ε show that phase shift defects first appear near the triangle apex for sufficiently low values of ε/kT (Figure 5c). Since lower values of ε/kT correspond to weaker intermolecular interactions, the model implies that phase shift defects only occur for relatively weak intermolecular interactions. Furthermore, lower ε/kT values can be interpreted as higher temperatures, thus confirming the thermodynamic stability of phase shift defects in confined spaces. Overall, the simulations agree well with the experimental observations, and seem to

confirm the assumption that lateral confinement leads to suppressed lamellar order as a result of a competition between molecule-substrate and molecule-molecule interactions.

Conclusions

In conclusion, we have shown how 2D lateral confinement impacts the formation of n-$C_{50}H_{102}$ assemblies at the solution-solid interface. Nanocorrals of various shapes were created on CM-HOPG *via* STM-based nanoshaving, and qualitative analysis revealed the suppression of lamellar order in response to geometric frustration. These results can be explained on the basis of competing enthalpic contributions from molecule-substrate and molecule-molecule interactions. The remarkable efficiency with which n-$C_{50}H_{102}$ assemblies adapt to the host nanocorral geometry follows from the lack of strong, directional intermolecular interactions. Furthermore, in line with previous *in situ* nanoshaving experiments, a strong molecular alignment effect is observed, which suggests that this effect is more generally applicable to linear, alkylated molecules. This work unites bottom-up and top-down approaches for surface functionalization, and exposes the role of spatial confinement on molecular ordering processes at the nanoscale. The analogy to results on 3D crystallization of alkanes in confined spaces highlights the utility of this method to be used as a well-defined model system to study self-assembly under confinement conditions. In addition, the combination of bottom-up and top-down techniques offers new possibilities for surface patterning. Extending this method to other surfaces and molecular systems is expected to advance the development and manipulation of novel functional materials at the molecular level.

Acknowledgements

This work is supported by the Fund of Scientific Research – Flanders (FWO), in part by FWO under EOS 30489208, and Internal Funds KU Leuven. L. V. thanks the FWO for the fellowship received. B. H. acknowledges the Belgian American Educational Foundation and the FWO.

Supporting information description

Cyclic voltammogram, additional STM images, statistical analyses.

References

1. Diao, Y.; Helgeson, M. E.; Myerson, A. S.; Hatton, T. A.; Doyle, P. S.; Trout, B. L. Controlled Nucleation from Solution Using Polymer Microgels. *J. Am. Chem. Soc.* **2011,** 133, 3756-3759.

2. Diao, Y.; Harada, T.; Myerson, A. S.; Hatton, T. A.; Trout, B. L. The Role of Nanopore Shape in Surface-Induced Crystallization. *Nat. Mater.* **2011,** 10, 867-871.

3. Jiang, Q.; Hu, C. H.; Ward, M. D. Stereochemical Control of Polymorph Transitions in Nanoscale Reactors. *J. Am. Chem. Soc.* **2013,** 135, 2144-2147.

4. Graubner, G.; Rengarajan, G. T.; Anders, N.; Sonnenberger, N.; Enke, D.; Beiner, M.; Steinhart, M. Morphology of Porous Hosts Directs Preferred Polymorph Formation and Influences Kinetics of Solid/Solid Transitions of Confined Pharmaceuticals. *Cryst. Growth Des.* **2014,** 14, 78-86.

5. Rengarajan, G. T.; Enke, D.; Steinhart, M.; Beiner, M. Size-Dependent Growth of Polymorphs in Nanopores and Ostwald's Step Rule of Stages. *Phys. Chem. Chem. Phys.* **2011,** 13, 21367-21374.

6. Hamilton, B. D.; Weissbuch, I.; Lahav, M.; Hillmyer, M. A.; Ward, M. D. Manipulating Crystal Orientation in Nanoscale Cylindrical Pores by Stereochemical Inhibition. *J. Am. Chem. Soc.* **2009,** 131, 2588-2596.

7. Henschel, A.; Kumar, P.; Hofmann, T.; Knorr, K.; Huber, P. Preferred Orientation of n-Hexane Crystallized in Silicon Nanochannels: A Combined X-ray Diffraction and Sorption Isotherm Study. *Phys. Rev. E* **2009,** 79, 032601.

8. Shimizu, S.; Agrawal, K. V.; O'Mahony, M.; Drahushuk, L. W.; Manohar, N.; Myerson, A. S.; Strano, M. S. Understanding and Analyzing Freezing-Point Transitions of Confined Fluids within Nanopores. *Langmuir* **2015,** 31, 10113-10118.

9. Hamilton, B. D.; Ha, J. M.; Hillmyer, M. A.; Ward, M. D. Manipulating Crystal Growth and Polymorphism by Confinement in Nanoscale Crystallization Chambers. *Acc. Chem. Res.* **2012,** 45, 414-423.

10. Maheshwari, P.; Dutta, D.; Sharma, S. K.; Sudarshan, K.; Pujari, P. K.; Majumder, M.; Pahari, B.; Bandyopadhyay, B.; Ghoshray, K.; Choshray, A. Effect of Interfacial Hydrogen Bonding on the Freezing/Melting Behavior of Nanoconfined Liquids. *J. Phys. Chem. C* **2010,** 114, 4966-4972.

11. Vartak, S.; Dwyer, L. M.; Myerson, A. S. Surface Functionalization in Combination with Confinement for Crystallization from Undersaturated Solutions. *CrystEngComm* **2018,** 20, 6136-6139.

12. de Oteyza, D. G.; Barrena, E.; Dosch, H.; Wakayama, Y. Nanoconfinement Effects in the Self-Assembly of Diindenoperylene (DIP) on Cu(111) Surfaces. *Phys. Chem. Chem. Phys.* **2009,** 11, 8741-8744.

13. Patrick, D. L.; Cee, V. J.; Beebe, T. P. Molecule Corrals for Studies of Monolayer Organic Films. *Science* **1994,** 265, 231-234.

14. Hooks, D. E.; Yip, C. M.; Ward, M. D. Nanoconfined Electrochemical Nucleation of Crystalline Molecular Monolayers on Graphite Substrates. *J. Phys. Chem. B* **1998,** 102, 9958-9965.

15. Xu, S.; Liu, G. Y. Nanometer-Scale Fabrication by Simultaneous Nanoshaving and Molecular Self-Assembly. *Langmuir* **1997,** 13, 127-129.

16. Takajo, D.; Nemoto, T.; Kurata, H.; Isoda, S.; Ozaki, H.; Mazaki, Y. Replacement of Molecules at Liquid/Solid Interfaces. *Thin Solid Films* **2003,** 438, 428-432.

17. Scudiero, L.; Hipps, K. W. Controlled Manipulation of Self-Organized Ni(II)-Octaethylporphyrin Molecules Deposited from Solution on HOPG with a Scanning Tunneling Microscope. *J. Phys. Chem. C* **2007,** 111, 17516-17520.

18. Greenwood, J.; Phan, T. H.; Fujita, Y.; Li, Z.; Ivasenko, O.; Vanderlinden, W.; Van Gorp, H.; Frederickx, W.; Lu, G.; Tahara, K.; Tobe, Y.; Uji-i, H.; Mertens, S. F. L.; De Feyter, S. Covalent Modification of Graphene and Graphite Using Diazonium Chemistry: Tunable Grafting and Nanomanipulation. *ACS Nano* **2015,** 9, 5520-5535.

19. Verstraete, L.; Greenwood, J.; Hirsch, B. E.; De Feyter, S. Self-Assembly under Confinement: Nanocorrals for Understanding Fundamentals of 2D Crystallization. *ACS Nano* **2016,** 10, 10706-10715.

20. Verstraete, L.; Smart, J.; Hirsch, B. E.; De Feyter, S. Unidirectional Supramolecular Self-Assembly inside Nanocorrals via in situ STM Nanoshaving. *Phys. Chem. Chem. Phys.* **2018,** 20, 27482-27489.

21. Seibel, J.; Verstraete, L.; Hirsch, B. E.; Bragança, A. M.; De Feyter, S. Biasing Enantiomorph Formation via Geometric Confinement: Nanocorrals for Chiral Induction at the Liquid-Solid Interface. *J. Am. Chem. Soc.* **2018,** 140, 11565-11568.

22. Hu, Y.; Braganca, A. M.; Verstraete, L.; Ivasenko, O.; Hirsch, B. E.; Tahara, K.; Tobe, Y.; De Feyter, S. Phase Selectivity Triggered by Nanoconfinement: the Impact of Corral Dimensions. *Chem. Commun.* **2019,** 55, 2226-2229.

23. Rabe, J. P.; Buchholz, S. Commensurability and Mobility in 2-Dimensional Molecular Patterns on Graphite. *Science* **1991,** 253, 424-427.

24. Marchenko, A.; Cousty, J.; Van, L. P. Magic Length Effects in the Packing of n-Alkanes Adsorbed on Au(111). *Langmuir* **2002,** 18, 1171-1175.

25. Hosoi, Y.; Sakurai, Y.; Yamamoto, M.; Ishii, H.; Ouchi, Y.; Seki, K. Structures of a Film of The Long-Chain n-Alkane n-C44H90 on a Cu(100) Surface. *Surf. Sci.* **2002,** 515, 157-174.

26. Cincotti, S.; Rabe, J. P. Self-Assembled Alkane Monolayers on MoSe2 and MoS2. *Appl. Phys. Lett.* **1993,** 62, 3531-3533.

27. Groszek, A. J. Selective Adsorption at Graphite/Hydrocarbon Interfaces. *Proc. Roy. Soc. Lond. A* **1970,** 314, 473-498.

28. Chen, Q.; Yan, H. J.; Yan, C. J.; Pan, G. B.; Wan, L. J.; Wen, G. Y.; Zhang, D. Q. STM Investigation of the Dependence of Alkane and Alkane (C18H38, C19H40) Derivatives Self-Assembly on Molecular Chemical Structure on HOPG Surface. *Surf. Sci.* **2008,** 602, 1256-1266.

29. Lopatina, Y. Y.; Marchenko, A. A. Adsorption of Hexacontane on Atomically-Flat Surfaces of Graphite and Au(111). *Thin Solid Films* **2018,** 665, 164-167.

30. Piot, L.; Marchenko, A.; Wu, J. S.; Mullen, K.; Fichou, D. Structural Evolution of Hexa-peri-hexabenzocoronene - Adlayers in Heteroepitaxy on n-Pentacontane Template Monolayers. *J. Am. Chem. Soc.* **2005,** 127, 16245-16250.

31. Rohr, C.; Gambra, M. B.; Gruber, K.; Hohl, C.; Malarek, M. S.; Scherer, L. J.; Constable, E. C.; Franosch, T.; Hermann, B. A. Predicting the Influence of a p2-Symmetric Substrate on Molecular Self-Organization with an Interaction-Site Model. *Chem. Commun.* **2011,** 47, 1800-1802.

32. Li, Z.; Van Gorp, H.; Walke, P.; Phan, T. H.; Fujita, Y.; Greenwood, J.; Ivasenko, O.; Tahara, K.; Tobe, Y.; Uji-I, H.; Mertens, S. F. L.; De Feyter, S. Area-Selective Passivation of sp(2) Carbon Surfaces by Supramolecular Self-Assembly. *Nanoscale* **2017,** 9, 5188-5193.

33. Tahara, K.; Ishikawa, T.; Hirsch, B. E.; Kubo, Y.; Brown, A.; Eyley, S.; Daukiya, L.; Thielemans, W.; Li, Z.; Walke, P.; Hirose, S.; Hashimoto, S.; De Feyter, S.; Tobe, Y. Self-Assembled Monolayers as Templates for Linearly Nanopatterned Covalent Chemical Functionalization of Graphite and Graphene Surfaces. *ACS Nano* **2018,** 12, 11520-11528.

34. Zhang, H. M.; Xie, Z. X.; Mao, B. W.; Xu, X. Self-Assembly of Normal Alkanes on the Au(111) Surfaces. *Chem. -Eur. J.* **2004,** 10, 1415-1422.

35. Arnold, T.; Thomas, R. K.; Castro, M. A.; Clarke, S. M.; Messe, L.; Inaba, A. The Crystalline Structures of the Even Alkanes Hexane, Octane, Decane, Dodecane and Tetradecane Monolayers Adsorbed on Graphite at Submonolayer Coverages and from the Liquid. *Phys. Chem. Chem. Phys.* **2002,** 4, 345-351.

36. Zhao, M.; Jiang, P.; Deng, K.; Yu, A. F.; Hao, Y. Z.; Xie, S. S.; Sun, J. L. Insight into STM Image Contrast of n-Tetradecane and n-Hexadecane Molecules on Highly Oriented Pyrolytic Graphite. *Appl. Surf. Sci.* **2011,** 257, 3243-3247.

37. Endo, O.; Ozaki, H.; Sumii, R.; Amemiya, K.; Nakamura, M.; Kosugi, N. Orientation of n-Alkane in Thin Films on Graphite (0001) Studied Using C K-NEXAFS. *J. Electron Spectrosc. Relat. Phenom.* **2011,** 184, 257-260.

38. Wang, L. P.; Sui, J.; Zhai, M.; Tian, F.; Lan, X. Z. Physical Control of Phase Behavior of Hexadecane in Nanopores. *J. Phys. Chem. C* **2015,** 119, 18697-18706.

39. Huber, P.; Soprunyuk, V. P.; Knorr, K. Structural Transformations of Even-Numbered n-Alkanes Confined in Mesopores. *Phys. Rev. E* **2006,** 74, 031610.

40. Pallaka, M. R.; Unruh, D. K.; Simon, S. L. Melting Behavior of n-Alkanes in Anodic Aluminum Oxide (AAO) Nanopores Using Flash Differential Scanning Calorimetry. *Thermochim. Acta* **2018,** 663, 157-164.

41. Okazaki, M.; Toriyama, K.; Anandan, S. Dynamics and Packing Mode of Long-Chained n-Alkane Molecules in the Nano-Channel of MCM-41. *Chem. Phys. Lett.* **2005,** 401, 363-367.

42. Xie, B. Q.; Shi, H. F.; Jiang, S. C.; Zhao, Y.; Han, C. C.; Xu, D. F.; Wang, D. J. Crystallization Behaviors of n-Nonadecane in Confined Space: Observation of Metastable Phase Induced by Surface Freezing. *J. Phys. Chem. B* **2006,** 110, 14279-14282.

43. Xie, B. Q.; Liu, G. M.; Jiang, S. C.; Zhao, Y.; Wang, D. J. Crystallization Behaviors of n-Octadecane in Confined Space: Crossover of Rotator Phase from Transient to Metastable Induced by Surface Freezing. *J. Phys. Chem. B* **2008,** 112, 13310-13315.

44. Jiang, K.; Su, Y. L.; Xie, B. Q.; Meng, Y. F.; Wang, D. J. Suppression of the Phase Separation in Binary n-Alkane Solid Solutions by Geometrical Confinement. *J. Phys. Chem. B* **2009,** 113, 3269-3272.

Table of contents